

# Mathematical Modelling of Neuroblast Migration towards the Olfactory Bulb

Daniel Acosta Soba  
 Carmen Castro González  
 Noelia Geribaldi Doldán  
 Francisco Guillén González  
 Pedro Núñez Abades  
 Noelia Ortega Román  
 Patricia Pérez García  
 J. Rafael Rodríguez Galván

January 16, 2023

## Abstract

This article is devoted to the mathematical modeling of migration of neuroblasts, precursor cells of neurons, along the pathway they usually follow before maturing. This pathway is determined mainly by attraction forces, to the olfactory bulb, and the heterogeneous mobility of neuroblasts in different regions of the brain. In numerical simulations, the application of novel discontinuous Galerkin methods allows to maintain the properties of the continuous model such as the maximum principle. We present some successful computer tests including parameter adjustment to fit real data from rodent brains.

## 1 Introduction

New neurons are generated in the adult rodent brain in specialized regions in which neural stem cells (NSC) are activated to produce neurons in a hierarchical process named neurogenesis. One of these regions is the subventricular zone (SVZ) [OAB19]. Activation of NSC induce their cell cycle entrance and posterior division to produce transit amplifying actively dividing progenitors that will give rise to neuronal progenitors or neuroblasts [CSVP<sup>14</sup>]. Newly generated neuroblasts migrate from the SVZ toward the olfactory bulb (OB) through the rostral migratory stream while still dividing [POAB13] contributing to the continuous neuronal replacement in the OB. Neurons produced in this homeostatic mechanisms integrate into existing circuits and participate in olfaction [LL11].

Tens of thousands of neuroblasts migrate daily through the RMS travelling long distances toward the OB, where they integrate as inhibitory interneurons [LAB94] [Alt69] [MvdK92] [CPL<sup>03</sup>]. These cells display an exploratory pattern while moving long distances [NKG<sup>07</sup>]. On this way along the adult RMS, neuroblasts border the corpus callosum (CC), a bundle of nerve fibers located between the left and right cerebral hemispheres, where the movement of neuroblasts is hindered due to the presence of a glial sheath delimiting the RMS and the low density of blood vessels in the CC, which they use as scaffold [LMAB<sup>12</sup>].

The importance of the homeostatic migration of neuroblasts toward the OB in the adult brain is highlighted by the fact that in models of brain damage an altered migration pattern is found. Several models of brain damage show an altered migration of SVZ neuroblasts that are different depending on the type of damage. Thus, in a murine model of Alzheimer's disease the proportion of migrating cells in the RMS is lower than in healthy mice [EMNG<sup>22</sup>] whereas in other models, such as murine models of Huntington's disease migration toward the OB is reduced as well accompanied by an altered pattern of migration that direct neuroblasts toward the striatum avoiding the OB pathway [KRA<sup>10</sup>] [KRW<sup>15</sup>]. Alterations of neuroblast migration are also observed in cortical injuries generated by ischemic lesions, in which SVZ neurogenesis is stimulated in response to the injury and in some cases chains of neuroblast can be seen migrating toward the injured region [MLM00].

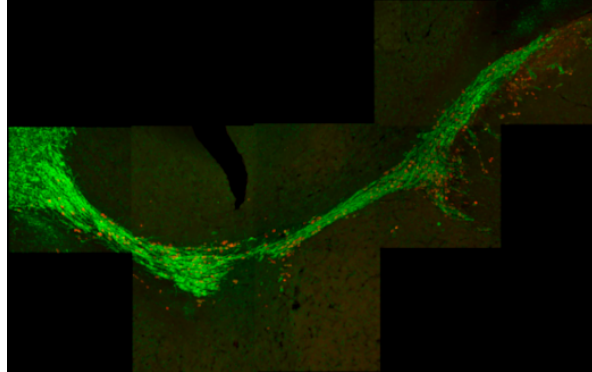


Figure 1: Original image, obtained from real data, showing neuroblast distribution in a rodent brain.

All these reports suggest that stimulating neurogenesis in the SVZ and conducting neuroblasts toward the injured region may be of use at designing strategies to regenerate damaged brain regions. Notwithstanding, although neurogenesis and neuroblast migration in the adult brain of mammals has been studied in depth over the past two decades from an anatomical and physiological point of view, and despite the considerable amount of data available over the years, up to our knowledge no mathematical or computational model has been published to date describing the neuroblast migration toward the OB. This type of models could be of great value as a first approximation to describe more complex phenomena, such as the movement of neuroblasts towards brain lesions.

In this paper we present a mathematical model of neuroblast migration to the olfactory bulb, based on the following hypothesis: the movement of neuroblasts is due to a transport phenomenon exerted by certain attraction or *chemotaxis* velocity towards the OB. More specifically, we suppose that there exists a function to be identified whose gradient drive the transport of neuroblasts. One of our main tasks in this work will be the correct modeling and numerical computing of this olfactory bulb function, which is defined along the brain and whose isolines reproduce the RMS path around the CC.

Once identified the transport velocity, we compute the migration of neuroblasts along the brain domain as solution of a convection PDE. It is well known that computing of numerical solutions to this kind of hyperbolic PDE equations is not an easy task [EG10, QSS10]. Fortunately we can successfully apply the upwind Discontinuous Galerkin (DG) techniques published in [ASGGRG22] to obtain quite appropriate results. The PDE is supplemented with some extra reaction terms described below, modelling the born of neuroblasts and their disappearance due to evolution in mature neurons.

Altough technically not of chemotaxis type, our model in inspired by chemotactic biological processes through which a population of organisms (or cells) migrate in response to a chemical stimulus. More specifically the study of cell motion affected by a chemical gradient, which results in net propagation up a chemoattractant gradient or down a chemorepellent gradient. Since the classical mathematical model, introduced in the 70's by E.F. Keller and L.A. Segel [KS70, KS71] the topic has aroused considerable interest in the mathematical community and many related variants have been proposed (see e.g. [BBTW15] for a review).

Finally, one of the main contributions in this work is the following: our mathematical model for neuroblast migration in the mammalian brain not only has been implemented in the computer, but it also has been calibrated and validated experimentally from previous real data we have experimentally obtained. This real neuroblasts distribution is identified in experimental images of the rodent brain as the red spots in Figure 1. They are specifically neuroblasts marked with the bromodeoxyuridine (BrdU), which indicates the dividing cells at the time of the injection. We can adjust the parameters of our model so that the solution match not only qualitatively, but quantitatively the experimental counting in these real images of the brain.

## 2 The neuroblast model

In this section, we present a model for migration of neuroblasts towards the OB along the RMS, starting from the SVZ and rounding the CC. Our more relevant hypothesis is the fact that the shape of this RMS path can be modeled by means of a attraction function which must be carefully designed.

Going into details, let us fix a space-time domain  $\Omega \times (0, T)$ , where  $\Omega \subset \mathbb{R}^2$ , is an open set representing a rodent brain, with boundary  $\partial\Omega$ . We consider the following PDE for  $u = u(\mathbf{x}, t) \geq 0$  the density of neuroblasts,

$$\tau u_t + \chi \nabla \cdot (u \nabla \mathcal{O}) + \alpha u - \gamma u \mathbb{1}_{NZ} = \beta \mathbb{1}_{SVZ} \quad \text{in } \Omega \times [0, T], \quad (1)$$

where  $\mathcal{O} = \mathcal{O}(\mathbf{x}) \in \mathbb{R}$  is a potential function such that its gradient  $\nabla \mathcal{O}$  models the attraction exerted by the olfactory bulb. The precise definition of this function  $\mathcal{O}$ , reflecting the heterogeneity of the brain with respect to the neuroblast migration, is detailed in Section 2.1 below. In any case,  $\mathcal{O}$  depends on a parameter  $\sigma > 0$ , related to the spread of neuroblasts along the domain. On the other hand, the parameter  $\chi > 0$  is the amplitude of this attraction,  $\alpha > 0$  is the death rate along the domain and  $\beta > 0$  is related to the amount of neuroblasts which are generated in the SVZ. Also a source term, with coefficient  $\gamma > 0$ , has been added intended to model a narrowing zone (NZ) in the brain, where some neuroblast contribution occurs in our 2d domain arising from other regions in the real 3d domain. Finally, the parameter  $\tau \in \{0, 1\}$  distinguishes the stationary and evolution cases, respectively.

Equation (1) is supplemented with the initial condition

$$u(0) = u^0 \quad \text{in } \Omega, \quad (2)$$

where  $u^0$ , the initial density of neuroblasts which will be obtained experimentally (see Section 4). Since we consider neuroblasts cannot cross the brain boundary, we must choice  $\mathcal{O}$  such that there is not entrance boundary, which mathematically means

$$\nabla \mathcal{O} \cdot \mathbf{n} \geq 0 \quad \text{on } \partial\Omega,$$

where  $\mathbf{n}$  is the exterior unit normal vector  $\partial\Omega$ .

### 2.1 Olfactory bulb chemoattraction

The attraction due to the olfactory bulb is computed in terms of a function,  $\mathcal{O} = \mathcal{O}(\mathbf{x}) \geq 0$ , which is obtained as the weak solution to a steady problem with reaction and anisotropic diffusion. This "olfactory bulb function" reaches its maximum at some given point  $(x_{\mathcal{O}}, y_{\mathcal{O}})$ , which stands for the center point of the Olfactory Bulb. Moreover  $\mathcal{O}$  will decrease homogeneously along  $\Omega$ , except in an certain area, the corpus callosum (CC), where the gradient of  $\mathcal{O}$  vanishes.

In order to obtain a function with the above-mentioned characteristics, we proceed as follows. Let  $CC \subset \Omega$  an open set defining the CC. We define the following expression which will be an anisotropic diffusion coefficient:

$$\mu_{CC} = \begin{cases} \frac{1}{\mu_P} & \text{in } CC, \\ \mu_P & \text{otherwise.} \end{cases} \quad (3)$$

The parameter  $\mu_P$  is *small permeability* positive value,  $\mu_P \in (0, 1)$ ,  $\mu_P \ll 1$ . The idea is to assign a huge diffusion number,  $\frac{1}{\mu_P} \gg 0$ , to the  $CC$ , while a vanishing diffusion to the rest of the mouse brain.

On the other hand, we consider following source term, defined as a Gaussian bell centered at the middle point of the olfactory bulb:

$$f_{\mathcal{O}}(x, y) = f_{\mathcal{O}}(\sigma; x, y) = e^{((x-x_{\mathcal{O}})^2 + (y-y_{\mathcal{O}})^2)/\sigma^2}. \quad (4)$$

The constant  $\sigma > 0$  is one of the key parameters in our model, determining the spread of the attraction of the OB along the brain and therefore the migration speed of neuroblasts in each point of  $\Omega$ . It will be estimated from real data by the process described in the following sections.

With all the above, we define  $\mathcal{O} \in H^1(\Omega)$  as the solution to

$$\begin{cases} \mathcal{O} - \nabla \cdot (\mu_{CC} \nabla \mathcal{O}) = f_{\mathcal{O}} & \text{in } \Omega, \\ \mathcal{O} = f_{\mathcal{O}} & \text{on } \partial\Omega. \end{cases} \quad (5)$$

The huge weight of the coefficient  $\mu_{CC}$  in the corpus callosum CC will make the solution  $\mathcal{O}$  to take a practically constant value in that area. Therefore  $\nabla \mathcal{O}$  will be very small in this region, so that migration of neuroblasts, defined by equation (1), is negligible inside the CC. Whereas in the remaining domain, the vanishing viscosity considered in (3) makes the solution behave like the anisotropic Gaussian function  $f_{\mathcal{O}}$  and thus the movement of neuroblasts acts according to the gradient of  $f_{\mathcal{O}}$  towards the center of the OB. Notice that we are considering this attraction independent of the time.

## 2.2 Initial condition

Equation (1)–(2) defines the migration of neuroblasts in  $\Omega$  for any initial condition  $u_0$ . But for testing realistic approximations of neuroblasts in Section 4, we must define  $u_0$  to match as closely as possible to experimental picture such as Figure 1, obtained from real data. Specifically, our aim is to define the initial neuroblasts distribution  $u_0$  as close as possible to the distribution of the red spots in Figure 1. They are neuroblasts marked with bromodeoxyuridine (BrdU), which indicates the dividing cells at the time of the injection of BrdU. Considering that this red marking will endure over time, data on the migration of these neuroblasts can be described, to which our model shall conform as much as possible.

Taking this into account, we define  $u_0$  as the solution to the steady state to our neuroblast model (1) for  $\tau = 0$ . Then  $u_0$  defines the behavior of a migration process which is unchanging in time, in a dynamic equilibrium. Our tests in Section 4 show that this process lead to accurate solutions, subject to an adequate adjustment of the parameters of the steady equations. This parameter set will be defined as follows:

$$\Lambda = (\alpha, \beta, \gamma, \chi, \sigma) \in \mathbb{R}_+^5 \quad (6)$$

## 3 Numerical schemes

Let  $0 = t_0 < t_1 < \dots < t_M = T$  be an uniform partition of the time domain  $[0, T]$  with  $\Delta t = t_m - t_{m-1}$ . Given any scalar function  $v: \Omega \times [0, T] \rightarrow \mathbb{R}$  and an approximation  $v^m \approx v(\cdot, t_m)$ , we denote by  $\delta_t v^m = \frac{v^m - v^{m-1}}{\Delta t}$  the backward Euler time discretization.

Regarding the space discretization, we consider a shape-regular triangular mesh  $\mathcal{T}_h = \{K\}_{K \in \mathcal{T}_h}$  of size  $h$  over a bounded polygonal domain  $\Omega \subset \mathbb{R}^d$ . We define the approximation spaces of discontinuous,  $\mathbb{P}_k^{\text{disc}}(\mathcal{T}_h)$ , and continuous,  $\mathbb{P}_k^{\text{cont}}(\mathcal{T}_h)$ , finite element functions over  $\mathcal{T}_h$  whose restriction to  $K \in \mathcal{T}_h$  are polynomials of degree  $k \geq 0$ . Moreover, we note the set of edges or faces of  $\mathcal{T}_h$  by  $\mathcal{E}_h$ , which can be splitted as  $\mathcal{E}_h = \mathcal{E}_h^i \cup \mathcal{E}_h^b$  into the *interior edges*  $\mathcal{E}_h^i$  and the *boundary edges*  $\mathcal{E}_h^b$ . Now, we fix the following orientation for the unit normal vector  $\mathbf{n}_e$  associated to any edge  $e \in \mathcal{E}_h$  of the mesh  $\mathcal{T}_h$ :

- If  $e \in \mathcal{E}_h^i$  is shared by the elements  $K$  and  $L$ , i.e.  $e = \partial K \cap \partial L$ , then  $\mathbf{n}_e$  is exterior to  $K$  pointing to  $L$ .
- If  $e \in \mathcal{E}_h^b$ , then  $\mathbf{n}_e$  points outwards of the domain  $\Omega$ .

In addition, the *average*  $\{\cdot\}$  and the *jump*  $[\cdot]$  of a scalar function  $v$  on an edge  $e \in \mathcal{E}_h$  are defined as follows:

$$\{\{v\}\} := \begin{cases} \frac{v_K + v_L}{2} & \text{if } e \in \mathcal{E}_h^i, \\ v_K & \text{if } e \in \mathcal{E}_h^b \end{cases}, \quad [v] := \begin{cases} v_K - v_L & \text{if } e \in \mathcal{E}_h^i, \\ v_K & \text{if } e \in \mathcal{E}_h^b \end{cases}.$$

Finally, we set the following notation for the positive and negative parts of a scalar function  $v$ :

$$v_{\oplus} := \frac{|v| + v}{2} = \max\{v, 0\}, \quad v_{\ominus} := \frac{|v| - v}{2} = -\min\{v, 0\}, \quad v = v_{\oplus} - v_{\ominus}.$$

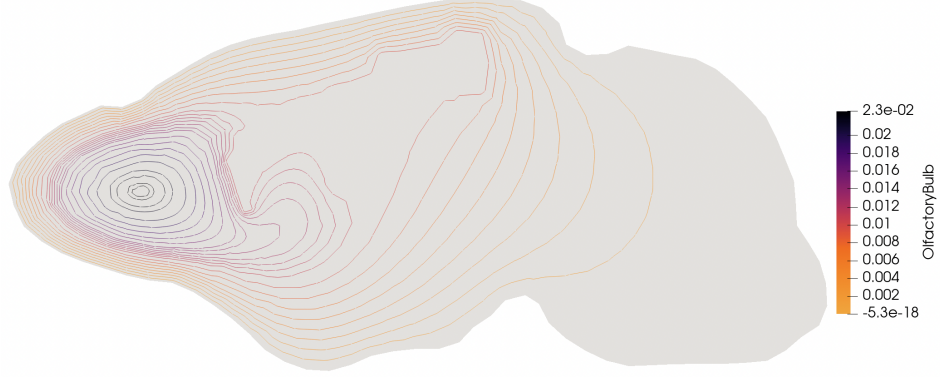


Figure 2: Isolines of the olfactory bulb attraction function, obtained with the parameters described in Section 4

### 3.1 Numerical approximation of the olfactory bulb attraction

We solve numerically the linear reaction-diffusion equation (5) in the domain defined by the mesh  $\mathcal{T}_h$  by using a  $P_1$ -continuous Finite Elements Method (FEM). Finally, the gradient of the this approximation of  $\mathcal{O}$  is computed and projected, again in a  $P_1$ -continuous FEM space. Before doing so, it will be necessary to identify those elements  $K \in \mathcal{T}_h$  laying in the CC, so that the anisotropic viscosity  $\mu_{CC}$  can be defined.

More in detail, given the parameter  $\sigma > 0$ , let  $f_{\mathcal{O}}$  the Gaussian bell introduced in in (4). Let us consider the problem:

$$\text{find } \mathcal{O} \in \mathbb{P}_1^{\text{cont}}(\mathcal{T}_h) \text{ such that } b(\mathcal{O}, \bar{\varphi}) = (f_{\mathcal{O}}, \bar{\varphi}), \quad \forall \bar{\varphi} \in \mathbb{P}_1^{\text{cont}}(\mathcal{T}_h), \quad (7)$$

where  $(\cdot, \cdot) = (\cdot, \cdot)_{L^2(\Omega)}$  stands for the scalar product in  $L^2(\Omega)$  and

$$b(\mathcal{O}, \bar{\varphi}) := \sum_{K \in \mathcal{T}_h} \int_K \mu_{CC} \nabla \mathcal{O} \cdot \nabla \bar{\varphi}.$$

The following result is derived from the Lax-Milgram Theorem.

**Proposition 3.1.** *For any constant  $\sigma > 0$ , there is a unique solution to the problem (7).*

The approximate solution  $\mathcal{O}$  thus obtained verifies the properties indicated in the Section 2.1, in particular it is increasing towards the OO and  $\nabla \mathcal{O}$  vanish in the CC. For a concrete example, obtained during the model adjustment in Section 4, see Figure 2.

### 3.2 Numerical solution of the neuroblasts model

Now we introduce the discrete schemes which have been used to approximate the neuroblasts migration model (1), either for the stationary case  $\tau = 0$  or for the evolution case. For the migration model, it is widely known (see e.g. [EG10, QSS10]) that FEM methods are not well suited for approximations to hyperbolic equations like (1), leading to the loss of its maximum principle property, spurious oscillations and wrong results. Here we will use an upwind discontinuous Galerkin method introduced in [ASGGRG22]. Before getting into the evolution problem, it will be essential to compute appropriate estimates to the olfactory bulb attraction function  $\mathcal{O}$  and to the initial condition  $u_0$ .

#### 3.2.1 Approximation of the initial condition

Let us consider a given set of parameters  $\Lambda = (\chi, \sigma, \alpha, \beta, \gamma) \in \mathbb{R}_+^5$  which will determine the initial condition  $u_0$ . We compute a piecewise constant approximation to  $u_0$  as the discontinuous Galerkin numerical solution to the steady ( $\tau = 0$ ) system (1) defined as follows. We consider the bilinear form

$$a_{\Lambda}(u, \bar{u}) := \chi a_h^{\text{upw}}(\nabla \mathcal{O}; u, \bar{u}) + \alpha (u, \bar{u}) - \gamma (u \mathbb{1}_{NZ}, \bar{u}) \quad (8)$$

where  $\mathcal{O} \in \mathbb{P}_1^{\text{cont}}(\mathcal{T}_h)$  is the solution to (7) for the parameter  $\sigma$  and  $a_h^{\text{upw}}(\cdot; \cdot, \cdot)$  is the upwind bilinear form discussed in [ASGGRG22] and defined as

$$a_h^{\text{upw}}(\boldsymbol{\mu}; v, \bar{v}) = - \sum_{K \in \mathcal{T}_h} \int_K v \boldsymbol{\mu} \cdot \nabla \bar{v} + \sum_{e \in \mathcal{E}_h^i, e=K \cap L} \int_e ((\boldsymbol{\mu} \cdot \mathbf{n}_e)_{\oplus} v_K - (\boldsymbol{\mu} \cdot \mathbf{n}_e)_{\ominus} v_L) \llbracket \bar{v} \rrbracket, \quad (9)$$

for any functions  $v, \bar{v}$  in the broken Sobolev space  $H^1(\mathcal{T}_h)$  and for any possibly discontinuous convective velocity field  $\boldsymbol{\mu} \in L^2(\mathcal{T}_h)^d$ . In the case of  $u, \bar{u} \in \mathbb{P}_0^{\text{disc}}(\mathcal{T}_h)$ , this bilinear form reduces to

$$a_h^{\text{upw}}(\boldsymbol{\mu}; u, \bar{u}) = \sum_{e \in \mathcal{E}_h^i, e=K \cap L} \int_e ((\boldsymbol{\mu} \cdot \mathbf{n}_e)_{\oplus} u_K - (\boldsymbol{\mu} \cdot \mathbf{n}_e)_{\ominus} u_L) \llbracket \bar{u} \rrbracket, \quad (10)$$

where in practice we will take  $\boldsymbol{\mu} = \nabla \mathcal{O}$ . Let us define the linear form on  $\mathbb{P}_0^{\text{disc}}(\mathcal{T}_h)$

$$L_{\Lambda}(\bar{u}) := \beta (\mathbb{1}_{\text{SVZ}}, \bar{u}) \quad (11)$$

and consider the problem: find  $u_0 \in \mathbb{P}_0^{\text{disc}}(\mathcal{T}_h)$  such that

$$a_{\Lambda}(u_0, \bar{u}) = L_{\Lambda}(\bar{u}), \quad \forall \bar{u} \in \mathbb{P}_0^{\text{disc}}(\mathcal{T}_h). \quad (12)$$

This problem has an unique of solution  $u_0 \in \mathbb{P}_0^{\text{disc}}(\mathcal{T}_h)$ , as stated in the Theorem 3.2 below. It will be selected as the initial condition for computing the numerical solution to the time dependent neuroblast model in the following section.

### 3.2.2 Numerical solution of the time-dependent neuroblasts model

Now, let us consider:

- A set of parameters  $\Lambda = (\chi, \sigma, \alpha, \beta, \gamma) \in \mathbb{R}_+^5$ .
- An approximation to the initial solution  $u_0 \in \mathbb{P}_0^{\text{disc}}(\mathcal{T}_h)$ , computed for a different set of parameters,  $\Lambda^0$ , as detailed in Section 3.2.1.
- A chemoattractant function  $\mathcal{O} \in \mathbb{P}_1^{\text{disc}}(\mathcal{T}_h)$ , defined as the solution to the olfactory bulb problem (7) depending on the parameter  $\sigma$ .

We approximate the solution of the evolution ( $\tau = 1$ ) system (1)–(2) using an implicit Euler time scheme and an upwind DG space discretization as follows. Let  $u^0 = u_0 \in \mathbb{P}_0^{\text{disc}}(\mathcal{T}_h)$ , for each  $m \in \mathbb{N}$ , given  $u^{m-1} \in \mathbb{P}_0^{\text{disc}}(\mathcal{T}_h)$ , find  $u^m \in \mathbb{P}_0^{\text{disc}}(\mathcal{T}_h)$  such that

$$(\delta_t u^m, \bar{u}) + a_{\Lambda}(u^m, \bar{u}) = L_{\Lambda}(\bar{u}), \quad \forall \bar{u} \in \mathbb{P}_1^{\text{disc}}(\mathcal{T}_h), \quad (13)$$

where  $a_{\Lambda}(\cdot, \cdot)$  is the bilinear form defined in (8). for the former parameter set  $\Lambda$ . In practice, we are going to take  $\beta = 0$ , that is no new neuroblasts are generated in the SVZ. The reason is that the unknown  $u^m$  represents the density of those neuroblasts which, at the initial time, were marked with BrdU. And no new marked neuroblasts appear in later times.

On the other hand, the linear form is defined for each time step as

$$L_{\Lambda}(\bar{u}) := \gamma \cdot (\mathbb{1}_{\text{NZ}} u^{m-1}, \bar{u}). \quad (14)$$

The proof of the following theorem easily follows from the results shown in Section 2.3 of [ASGGRG22].

#### Theorem 3.2.

1. There is a unique solution to the steady problem (12). This solution satisfies  $u_0 \geq 0$ .
2. There is a unique solution to the unsteady problem (13). This solution satisfies  $u^m \geq 0$ .

## 4 Adjustment of the model to real data

The numerical schemes described above have been applied to develop computer programs that allow solving the PDE model for simulation of migration of neuroblasts in the brain, yielding concrete data and comparing it to experimental data obtained from real rodent brains. The final target is calibrating the model parameters so that its output is matched as closely as possible to the real data.

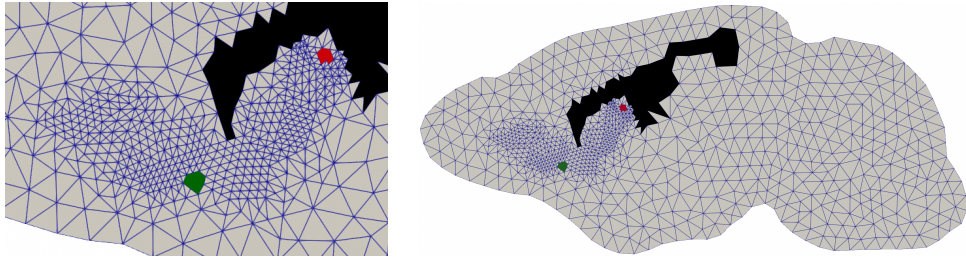


Figure 3: Right: mesh of a virtual rodent brain. Left: zoom around the RMS. Triangles defining the CC, SVZ and NZ are shown in black, red and green color, respectively

#### 4.1 Computer implementation in a realistic domain

For computer implementation of the schemes described in Section 3.2, we have defined a mesh of a virtual rodent brain, see Figure 3. In this mesh, the triangles that are located in the CC have been identified (they are shown in black color in Figure 3) and also those triangles laying in the SVZ and in the NZ (they are shown in color red and green, respectively, in Figure 3).

It is worth noting that the mesh shown in Figure 3 is actually the one resulting from refining and saving a coarser mesh that was initially built. Specifically, we build an initial mesh of the brain domain and then we refine it in the area where the RMS is expected to be located. We identify this area by a preliminary calculus of the initial solution  $u_0$ , then we refine those triangles where  $u_0 > \varepsilon$ , where  $\varepsilon$  is a prescribed small constant. Using this refined mesh allows us computing a more accurate solution for neuroblasts distribution in the region of interest, without significantly increasing the computational effort.

The final mesh we are using in our numerical tests,  $\mathcal{T}_h$ , is made of 2003 triangles with size  $h \in [3.313 \cdot 10^{-3}, 4.814 \cdot 10^{-2}]$ . For the time discretization, we define an uniform partition  $t_0 < \dots < t_m < \dots < t_M$  of the time interval  $[0, T]$  with  $T = 4$  days and constant size  $k = t_m - t_{m-1} = 0.04$ . We use the library *FEniCS* [ABH<sup>+</sup>15] to load the mesh, define the Galerkin spaces  $\mathbb{P}_1^{\text{cont}}(\mathcal{T}_h)$  and  $\mathbb{P}_0^{\text{disc}}(\mathcal{T}_h)$ , and finally we code the time advancing schemes detailed in Section 3. More in detail, considering the parameter set  $\Lambda$  as in 6:

1. For each olfactory bulb shape parameter  $\sigma$ , we compute the  $\mathbb{P}_1^{\text{cont}}(\mathcal{T}_h)$  solution  $\mathcal{O}$  to system (7), where the Gaussian RHS function  $f_{\mathcal{O}}$  depends on  $\sigma$  and where the anisotropic constant  $\mu_{CC}$  introduced in (3) is defined as constant tiny values on the triangles located in the CC. This olfactory bulb function  $\mathcal{O}$  is one of the keys in our model and will determine the migration of neuroblasts, driven by  $\nabla \mathcal{O}$  and thus orthogonal to the isolines of  $\mathcal{O}$  (see Figure 2).
2. Given an attraction function  $\mathcal{O}$  depending on parameter  $\sigma$  and given the positive parameters  $\alpha, \beta, \gamma, \chi$  (in the stationary case, one of them can be eliminated as in Section 4.3), an initial condition  $u_0 \in \mathbb{P}_0^{\text{disc}}(\mathcal{T}_h)$  can be computed solving problem (12). And then, for the same or different parameters, we can compute at each time step in  $t_m, m = 1, \dots, M$ , the neuroblast distribution  $u^m \in \mathbb{P}_0^{\text{disc}}(\mathcal{T}_h)$  solving (13).

#### 4.2 Computing optimal parameters

Although the process so far described is valid and has been successfully tested in qualitative tests, in what follows we will explore whether it is feasible to adjust the parameters to match the reality. We describe the process to obtain an optimal set of mathematical parameters  $\Lambda$  as in 6 so that the output of our model is in accordance to the experimental biological data described next.

In order to obtain a realistic experimental biological data set, we have labeled the RMS of two month-old adult male and female mice. The experimental design consisted on the labeling proliferating cells within the SVZ, RMS and OB using BrdU and analyzing the time employed by labeled neuroblasts to leave the RMS.

Among the available information we encounter the number of neuroblasts that were found in three different control regions. In order to make use of this information, a preliminary data analysis process

was carried out in which 13 objects were categorized as outliers and removed from the dataset. These outliers presented either an unusual position or surface of the control regions in the brain or an odd number of neuroblasts in these regions.

Finally, the mean of the data for the different mice/slices were computed. This way, our model is set to reproduce the quantitative and qualitative behaviour of the neuroblasts migration process in a mean transversal slice close to the center of a mean mouse brain, according to the available data.

Then we start from this data set obtained from manual recount of neuroblasts in images obtained from real rodent brains. Let us denote  $\hat{u}_i^m$  to the real counting of neuroblasts in the biological brain region  $\hat{B}_i$  at the time step  $t_m$ . We pretend to calculate an initial condition  $u_0$  and a parameter set  $\Lambda = (\alpha, \beta, \gamma, \chi, \sigma)$  minimizing the difference between the neuroblasts accounted in region  $\hat{B}_i$  and the output of our model in some predefined mathematical balls  $B_i \subset \Omega$ . For that, we consider the following error expression at the time  $t_m \in [0, T]$ :

$$E^m = E^m(\Lambda) = \frac{1}{N_x} \sum_{i=1}^{N_x} \frac{1}{(\hat{u}_i^m)^2} |u_i^m - \hat{u}_i^m|^2 \quad (15)$$

where

$$u_i^m = u_i^m(\Lambda) = \int_{B_i} u_h^m(x) dx$$

and  $u^m = u^m(\Lambda)$  is the approximate solution to equation (13) at time  $t_m$  for the parameter set  $\Lambda$ . Notice that the error  $E^0$  can be computed from the initial condition  $u_0$  (which is obtained from the steady equation (12) and normally from a different parameter set), because  $u_h^0 = u_0$ .

Let also consider the global error expression

$$E = E(\Lambda) = \frac{1}{N_T} \sum_{i=1}^{N_T} E^m = \frac{1}{N_T \cdot N_x} \sum_{m=1}^{N_T} \sum_{i=1}^{N_x} \frac{1}{(\hat{u}_i^m)^2} |u_i^m - \hat{u}_i^m|^2. \quad (16)$$

The process of parameters adjustment is split in two steps: first, we compute an optimal parameter set for the initial state,  $u_0$ , and then we calculate a second optimal parameter set for the evolution neuroblast model. For that purpose, two different techniques are applied: on the one hand, non-linear regression, which provides a preliminary parameters setting. And on the second hand, these preliminary values are optimized by minimizing the relative quadratic error between the real data and the one resulting from the numerical solution of our equation systems.

Here we describe the algorithms applied for obtaining optimal parameters: non-linear regression and optimization algorithm for minimizing the error.

## Regression

We use the SKLEARN library in PYTHON [PVG+11]. To obtain a better approximation for the initial vector of parameters, we apply non-linear regression, based on decision trees (with RANDOMFORESTREGRESSOR from SKLEARN.ENSEMBLE). The data needed to train the regressor consists on the values of the integrals in the balls and their correspondent parameters. It is written in csv files with the following format:

$$\Lambda = (\alpha, \beta, \gamma, \chi, \sigma)$$

Time \ Position	$B_1$	$B_2$	$B_3$
$t_0$	$\int_{B_1} u_h(x, t_0) dx$	$\int_{B_2} u_h(x, t_0) dx$	$\int_{B_3} u_h(x, t_0) dx$
$t_1$	$\int_{B_1} u_h(x, t_1) dx$	$\int_{B_2} u_h(x, t_1) dx$	$\int_{B_3} u_h(x, t_1) dx$
$t_2$	$\int_{B_1} u_h(x, t_2) dx$	$\int_{B_2} u_h(x, t_2) dx$	$\int_{B_3} u_h(x, t_2) dx$

Using the trained regressor, we can obtain a first approximation of the parameters by introducing the values of the integrals as shown in the previous table. For the steady problem, used to obtain the initial condition, we only need the first row of the table, which corresponds to the initial time. Then, the whole table is used to find the approximated parameters of the time evolution problem.

## Optimization

Finally, starting from the parameters we got with the regressor, we optimize them so the quadratic error between the real values of the integrals and the ones we obtain numerically is minimized. We use the `OPTIMIZE` library ([VGO<sup>+</sup>20]) with its L-BFGS-B method, which, in addition, allows us to set the bounds for the parameters if needed.

### 4.3 Initial condition: fitting real data

Firstly, we need to compute an approximation to the initial distribution of neuroblasts, which will be taken as the initial condition  $u_0$  of the evolution scheme. It is going to be computed as solution of the steady problem ( $\tau = 0$ ), for adequate values of the parameters  $\Lambda$ . In this case, to reduce the possibilities when looking for the optimal parameters, we are going to eliminate parameter  $\chi$  by dividing the equation 12 by it. This parameter is a good choice for division, because we assume (and our numerical tests confirm this assumption) that it cannot be too small. In fact, our steady equation is now:

$$a_h^{\text{upw}}(\nabla \mathcal{O}; u, \bar{v}) + \frac{\alpha}{\chi}(u, \bar{v}) - \frac{\beta}{\chi}(\mathbb{1}_{SVZ}, \bar{v}) = \frac{\gamma}{\chi}(\mathbb{1}_{NZ}, \bar{v}), \quad (17)$$

where  $\mathcal{O}$  is the solution to the olfactory bulb equation (7), which depends on the shape parameter  $\sigma$  through the source term for  $f_{\mathcal{O}}$ , according to (4).

Then, denoting the rescaled parameters as

$$\alpha' = \frac{\alpha}{\chi}, \quad \beta' = \frac{\beta}{\chi}, \quad \gamma' = \frac{\gamma}{\chi},$$

we focus on finding useful ranges where we get under and over approximation errors. Taking into account the positivity of the data, and also some previous qualitative numerical tests and other heuristic considerations we select the following intervals:

$$\alpha' \in [10^{-3}, 1], \quad \beta' \in [2.5, 20], \quad \gamma' \in [10^{-3}, 20].$$

Regarding the parameter  $\sigma$ , it has a different nature to  $\alpha$ ,  $\beta$  and  $\gamma$ , being more directly related to the spread along the domain of the OB. Since we are considering normalized dimensions for the domain, we take  $\sigma \in [0.2, 0.6]$ . Once the ranges of variation of the parameters have been fixed, we build a four dimensional grid with several values for each parameter.

Next, we proceed to solve the equation (17) for every parameters combinations and for each one we compute the error respect the following experimental values, extracted from an average of the manual recount of neuroblasts in real images: This way, we obtain the required data to train the Random

Time / Position	SVZ	RMS	OB
8h	9.8	24.2	8.4

Table 1: Real data for the initial condition

Forest Regressor.

Once finished the training process, we obtain a first approximation of the searched parameters:

$$\alpha' = 4.960, \quad \beta' = 3.311 \cdot 10^4, \quad \sigma = 1.0 \quad \text{and} \quad \gamma' = 8.668 \cdot 10^6.$$

Nevertheless, those parameters carry a big relative error. Before the optimization, we need to analyze the qualitative situation to adjust the parameters according to the physic phenomena. In sight of the Figure 4, we notice an excessive density of neuroblasts near the olfactory bulb. Therefore, we should decrease the parameter  $\sigma$  and remove  $\gamma'$ . Focusing now on the subventricular zone, we observe an incorrect phenomena: the born cells do not reach the full path, they seem to be degraded at the beginning. Thus, we need to reduce  $\alpha'$ . Also, to avoid the excessive accumulation of cells due to the new degradation parameter, we will reduce  $\beta'$ . Under the previous observations, we consider now:

$$\alpha' = 6.0 \cdot 10^{-1}, \quad \beta' = 1.7 \cdot 10^3, \quad \sigma = 7.5 \cdot 10^{-1} \quad \text{and} \quad \gamma' = 0.0.$$

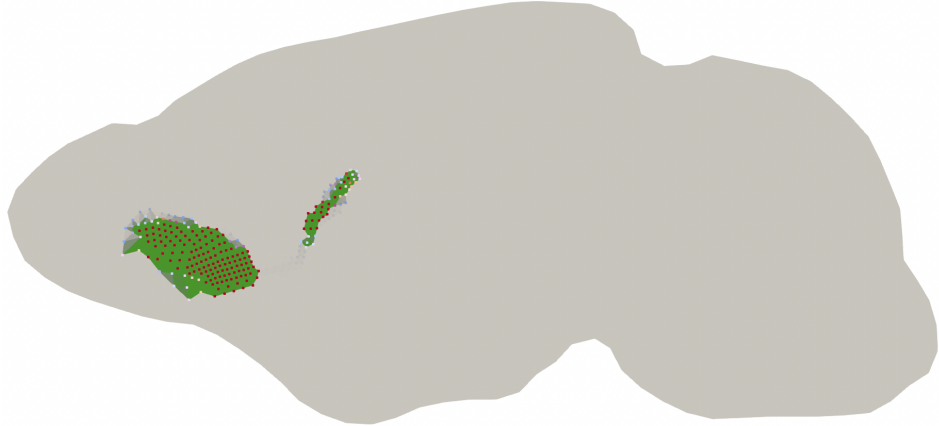


Figure 4: Numerical solution for the initial condition from regression parameters.

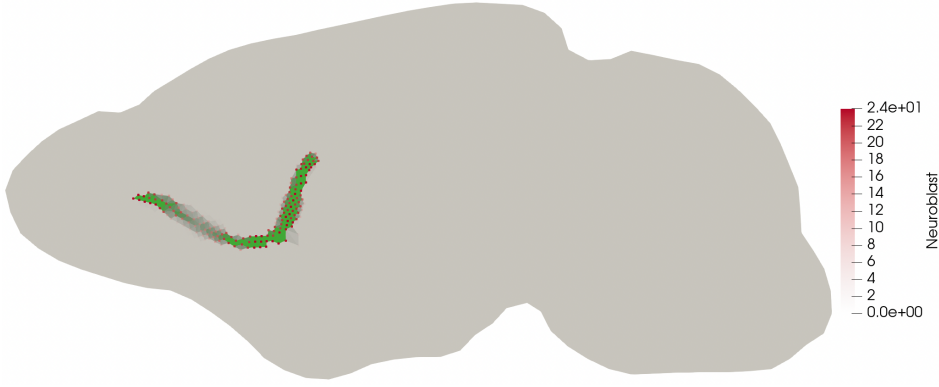


Figure 5: Steady neuroblast density from optimization

Finally, the optimal parameters are provided by the L-BFGS-B method, from the Optimize library. Setting a maximum number of iterations of  $10^3$ , we obtain the following parameters:

$$\alpha' = 9.069 \cdot 10^{-2}, \quad \beta' = 1.70 \cdot 10^3, \quad \sigma = 7.331 \cdot 10^{-1} \quad \text{and} \quad \gamma' = 0.0. \quad (18)$$

Now, the quadratic error is  $E = 0.001$ . And the results, as shown in Figures 2 and 5, agree with the real phenomena from Figure 6. Even more, the number of neuroblasts given by these parameters in each position (see Table 2) is can be considered as good results, especially if the huge variance of the

Time \ Position	SVZ	RMS	OB
8h	9.76	23.04	8.72

Table 2: Data produced by our model for the initial condition

experimental data is taken into consideration.

#### 4.4 Neuroblast evolution model: fitting real data

Now, starting from the initial solution  $u_0$  computed in previous section, we are going to find the parameters which make the evolution model fit the real data as much as possible. Unlike the stationary case, we cannot divide by  $\chi$  to reduce the parameter set when looking for the optimal parameters. But now we can consider the following fact: we are modeling those neuroblasts that, at the initial time, were marked with bromodeoxyuridine (BrdU), which are represented as red spots in Figure 1. Since no new neuroblasts will be marked in later times, we can set  $\beta = 0$ , neglecting the neuroblast birth term in the SVZ. Therefore we have again four parameters to fit and our numerical scheme can be

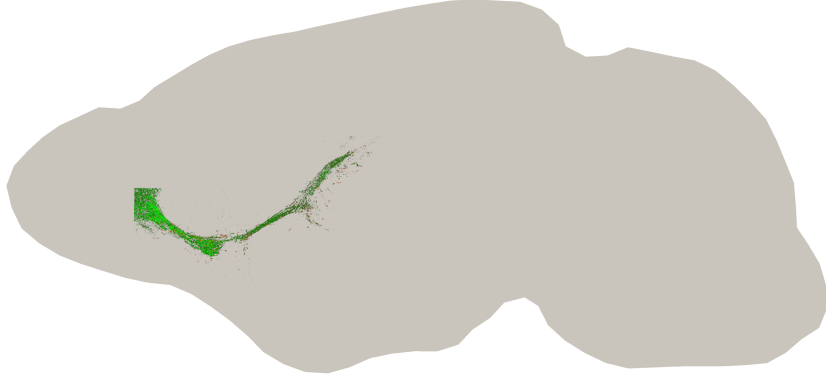


Figure 6: Real steady neuroblast density

detailed as:

$$(\delta_t u^m, \bar{u}) + \chi a_h^{\text{upw}}(\nabla \mathcal{O}; u^m, \bar{u}) + \alpha(u^m, \bar{u}) = \gamma(\mathbb{1}_{NZ} u^{m-1}, \bar{u}). \quad (19)$$

Therefore we build a three dimensional grid with several values for each parameter. The experimental values are shown in Table 3. After we trained the regressor as before, we obtain a first

Time \ Position	SVZ	RMS	OB
48h	0.25	13.5	52.7
96h	0.01	8.5	41.5

Table 3: Data produced by our neuroblast evolution model at the two final time steps

approximation of the searched parameters:

$$\alpha = 4.322 \cdot 10^{-2}, \quad \chi = 6.828 \cdot 10^3 \quad \sigma = 8.805 \cdot 10^2 \quad \text{and} \quad \gamma = 2.918.$$

Nevertheless, for those values the quadratic error obtained is:  $E = 0.439$ . As we did in the previous case, we change some parameters to be in accordance with the physical phenomena.

Specifically, considering the Olfactory Bulb attraction as immutable along the time, we can assume that  $\sigma$  is fixed to the value obtained for the stationary problem in the previous section,  $\sigma = 7.331 \cdot 10^{-1}$ . In fact, this a key constant, which models the spread of the olfactory bulb, and once computed it is not supposed to change. But, as we have decreased  $\sigma$ , we should increase  $\chi$  in order to maintain the same attraction force. However, this parameter was not in the previous case, so we will just consider  $\chi = 1.0$ . This way, our parameters are:

$$\alpha = 4.322 \cdot 10^{-2}, \quad \chi = 1.0 \quad \sigma = 7.331 \cdot 10^{-1} \quad \text{and} \quad \gamma = 2.918.$$

Finally, when we apply the L-BFGS-B method to optimize the error, under the same conditions as before, we obtain:

$$\alpha = 1.275 \cdot 10^{-1}, \quad \chi = 4989 \cdot 10^{-2} \quad \sigma = 7.339 \cdot 10^{-1} \quad \text{and} \quad \gamma = 3.496.$$

The quadratic error obtained now is:  $E = 0.011$ . At Figures 7 and 8, the neuroblasts migration is represented for the optimal parameters. The quadratic error for the whole simulation is:  $E = 0.008$ , and the number of neuroblasts in each position and time is:

Time \ Position	SVZ	RMS	OB
8h	9.76	23.04	8.72
48h	0.0	14.25	52.31
96h	0.0	8.22	41.76

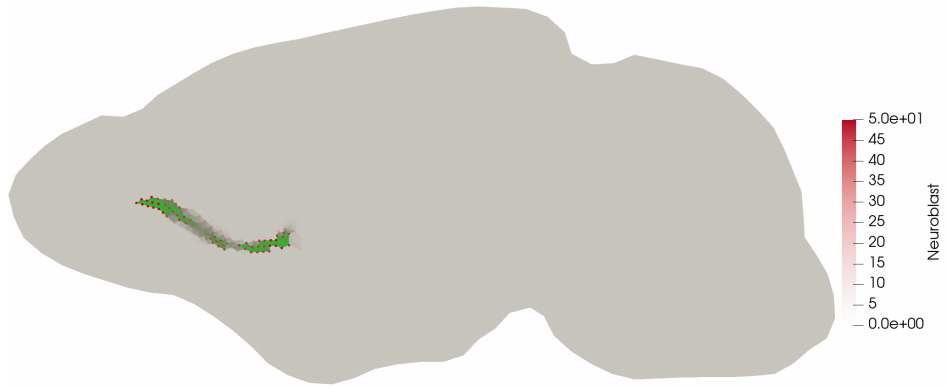


Figure 7: Evolution of neuroblast density after two days for the optimal parameters

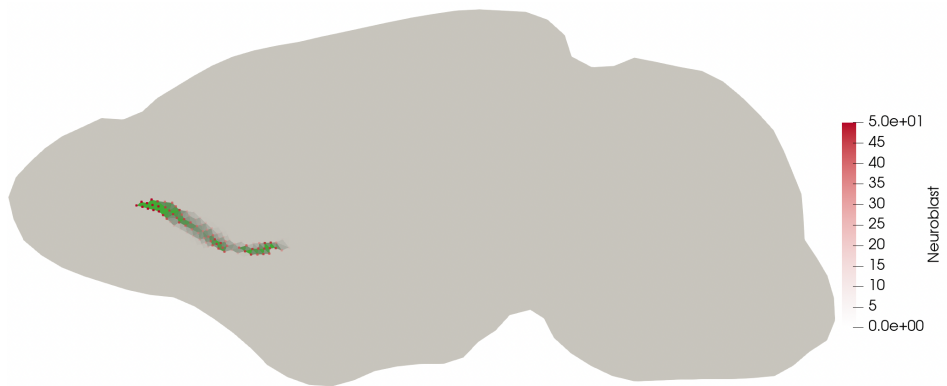


Figure 8: Evolution of neuroblast density after four days for the optimal parameters

## References

[ABH<sup>+</sup>15] Martin Alnæs, Jan Blechta, Johan Hake, August Johansson, Benjamin Kehlet, Anders Logg, Chris Richardson, Johannes Ring, Marie E Rognes, and Garth N Wells. The fenics project version 1.5. *Archive of Numerical Software*, 3(100), 2015.

[Alt69] J. Altman. Autoradiographic and histological studies of postnatal neurogenesis. iv. cell proliferation and migration in the anterior forebrain, with special reference to persisting neurogenesis in the olfactory bulb. *J Comp Neurol*, 137(4):433–57, 1969. Altman, J eng 1969/12/01 J Comp Neurol. 1969 Dec;137(4):433-57. doi: 10.1002/cne.901370404.

[ASGGRG22] Daniel Acosta-Soba, Francisco Guillén-González, and J. Rafael Rodríguez-Galván. An upwind DG scheme preserving the maximum principle for the convective Cahn–Hilliard model. *Numerical Algorithms*, August 2022.

[BBTW15] Nicola Bellomo, Abdelghani Bellouquid, Youshan Tao, and Michael Winkler. Toward a mathematical theory of Keller–Segel models of pattern formation in biological tissues. *Mathematical Models and Methods in Applied Sciences*, 25(09):1663–1763, May 2015.

[CPL<sup>+</sup>03] A. Carleton, L. T. Petreanu, R. Lansford, A. Alvarez-Buylla, and P. M. Lledo. Becoming a new neuron in the adult olfactory bulb. *Nat Neurosci*, 6(5):507–18, 2003. Carleton, Alan Petreanu, Leopoldo T Lansford, Rusty Alvarez-Buylla, Arturo Lledo, Pierre-Marie eng HD32116/HD/NICHD NIH HHS/ Research Support, Non-U.S. Gov’t Research Support, U.S. Gov’t, P.H.S. 2003/04/22 Nat Neurosci. 2003 May;6(5):507-18. doi: 10.1038/nn1048.

[CSVP<sup>+</sup>14] P. Codega, V. Silva-Vargas, A. Paul, A. R. Maldonado-Soto, A. M. Deleo, E. Pastrana, and F. Doetsch. Prospective identification and purification of quiescent adult neural stem cells from their in vivo niche. *Neuron*, 82(3):545–59, 2014. Codega, Paolo Silva-Vargas, Violeta Paul, Alex Maldonado-Soto, Angel R Deleo, Annina M Pastrana, Erika Doetsch, Fiona eng T32 MH 15174-29/MH/NIMH NIH HHS/ NS053884/NS/NINDS NIH HHS/ NS074039/NS/NINDS NIH HHS/ T32 GM007088/GM/NIGMS NIH HHS/ TL1 TR000082/TR/NCATS NIH HHS/ R01 NS053884/NS/NINDS NIH HHS/ F31 NS081990/NS/NINDS NIH HHS/ F31 NS079057/NS/NINDS NIH HHS/ NS053884-03S109/NS/NINDS NIH HHS/ T32 GM008224/GM/NIGMS NIH HHS/ T32 MH015174/MH/NIMH NIH HHS/ 1F31NS081990/NS/NINDS NIH HHS/ R01 NS074039/NS/NINDS NIH HHS/ 1F31NS079057/NS/NINDS NIH HHS/ Research Support, N.I.H., Extramural Research Support, Non-U.S. Gov’t 2014/05/09 Neuron. 2014 May 7;82(3):545-59. doi: 10.1016/j.neuron.2014.02.039.

[EG10] Alexandre Ern and Jean-Luc Guermond. *Theory and Practice of Finite Elements*. Number 159 in Applied mathematical sciences. Springer, 2010.

[EMNG<sup>+</sup>22] D. Esteve, M. M. Molina-Navarro, E. Giraldo, N. Martínez-Varea, M. C. Blanco-Gandia, M. Rodríguez-Arias, J. M. García-Verdugo, J. Vina, and A. Lloret. Adult neural stem cell migration is impaired in a mouse model of alzheimer’s disease. *Mol Neurobiol*, 59(2):1168–1182, 2022. Esteve, Daniel Molina-Navarro, Maria Micaela Giraldo, Esther Martínez-Varea, Noelia Blanco-Gandia, Mari-Carmen Rodríguez-Arias, Marta García-Verdugo, Jose Manuel Vina, Jose Lloret, Ana eng 696295/horizon 2020/ CB16/10/00435/instituto de salud carlos iii/ PID2019-110906RB-I00/ministerio de ciencia, innovacion y universidades/ PROMETEO/2019/097/conselleria de sanitat universal i salut publica/ 825546/joint programming initiative a healthy diet for a healthy life/ UV-INV-AE-1546096/Universitat de Valencia/ 2021/12/12 Mol Neurobiol. 2022 Feb;59(2):1168-1182. doi: 10.1007/s12035-021-02620-6. Epub 2021 Dec 11.

[KRA<sup>+</sup>10] Z. Kohl, M. Regensburger, R. Aigner, M. Kandasamy, B. Winner, L. Aigner, and J. Winkler. Impaired adult olfactory bulb neurogenesis in the r6/2 mouse model of huntington’s disease. *BMC Neurosci*, 11:114, 2010. Kohl, Zacharias Regensburger, Martin Aigner, Robert Kandasamy, Mahesh Winner, Beate Aigner, Ludwig Winkler, Jurgen

eng Research Support, Non-U.S. Gov't England 2010/09/15 *BMC Neurosci*. 2010 Sep 13;11:114. doi: 10.1186/1471-2202-11-114.

[KRW<sup>+</sup>15] M. Kandasamy, M. Rosskopf, K. Wagner, B. Klein, S. Couillard-Despres, H. A. Reitsamer, M. Stephan, H. P. Nguyen, O. Riess, U. Bogdahn, J. Winkler, S. von Horsten, and L. Aigner. Reduction in subventricular zone-derived olfactory bulb neurogenesis in a rat model of huntington's disease is accompanied by striatal invasion of neuroblasts. *PLoS One*, 10(2):e0116069, 2015. Kandasamy, Mahesh Rosskopf, Michael Wagner, Katrin Klein, Barbara Couillard-Despres, Sebastien Reitsamer, Herbert A Stephan, Michael Nguyen, Huu Phuc Riess, Olaf Bogdahn, Ulrich Winkler, Jurgen von Horsten, Stephan Aigner, Ludwig eng Research Support, Non-U.S. Gov't 2015/02/27 *PLoS One*. 2015 Feb 26;10(2):e0116069. doi: 10.1371/journal.pone.0116069. eCollection 2015.

[KS70] Evelyn F. Keller and Lee A. Segel. Initiation of slime mold aggregation viewed as an instability. *Journal of Theoretical Biology*, 26(3):399–415, March 1970.

[KS71] Evelyn F. Keller and Lee A. Segel. Model for chemotaxis. *Journal of Theoretical Biology*, 30(2):225–234, February 1971.

[LAB94] C. Lois and A. Alvarez-Buylla. Long-distance neuronal migration in the adult mammalian brain. *Science*, 264(5162):1145–8, 1994. Lois, C Alvarez-Buylla, A eng NS 24478/NS/NINDS NIH HHS/ Research Support, Non-U.S. Gov't Research Support, U.S. Gov't, P.H.S. 1994/05/20 *Science*. 1994 May 20;264(5162):1145-8. doi: 10.1126/science.8178174.

[LL11] F. Lazarini and P. M. Lledo. Is adult neurogenesis essential for olfaction? *Trends Neurosci*, 34(1):20–30, 2011. Lazarini, Francoise Lledo, Pierre-Marie eng Research Support, Non-U.S. Gov't Review England 2010/10/29 *Trends Neurosci*. 2011 Jan;34(1):20-30. doi: 10.1016/j.tins.2010.09.006. Epub 2010 Oct 25.

[LMAB<sup>+</sup>12] C. Le Magueresse, J. Alfonso, C. Bark, M. Eliava, S. Khrulev, and H. Monyer. Subventricular zone-derived neuroblasts use vasculature as a scaffold to migrate radially to the cortex in neonatal mice. *Cereb Cortex*, 22(10):2285–96, 2012. Le Magueresse, Corentin Alfonso, Julieta Bark, Christine Eliava, Marina Khrulev, Sergey Monyer, Hannah eng Research Support, Non-U.S. Gov't 2011/11/19 *Cereb Cortex*. 2012 Oct;22(10):2285-96. doi: 10.1093/cercor/bhr302. Epub 2011 Nov 17.

[MLM00] S. S. Magavi, B. R. Leavitt, and J. D. Macklis. Induction of neurogenesis in the neocortex of adult mice. *Nature*, 405(6789):951–5, 2000. Magavi, S S Leavitt, B R Macklis, J D eng Research Support, Non-U.S. Gov't Research Support, U.S. Gov't, P.H.S. England 2000/07/06 *Nature*. 2000 Jun 22;405(6789):951-5. doi: 10.1038/35016083.

[MvdK92] C. M. Morshead and D. van der Kooy. Postmitotic death is the fate of constitutively proliferating cells in the subependymal layer of the adult mouse brain. *J Neurosci*, 12(1):249–56, 1992. Morshead, C M van der Kooy, D eng Research Support, Non-U.S. Gov't 1992/01/01 *J Neurosci*. 1992 Jan;12(1):249-56. doi: 10.1523/JNEUROSCI.12-01-00249.1992.

[NKD<sup>+</sup>07] S. C. Nam, Y. Kim, D. Dryanovski, A. Walker, G. Goings, K. Woolfrey, S. S. Kang, C. Chu, A. Chenn, F. Erdelyi, G. Szabo, P. Hockberger, and F. G. Szele. Dynamic features of postnatal subventricular zone cell motility: a two-photon time-lapse study. *J Comp Neurol*, 505(2):190–208, 2007. Nam, Sang Chae Kim, Yongsoo Dryanovski, Dilyan Walker, Avery Goings, Gwendolyn Woolfrey, Kevin Kang, Seong Su Chu, Chris Chenn, Anjen Erdelyi, Ferenc Szabo, Gabor Hockberger, Philip Szele, Francis G eng R01 NS/AG42253/AG/NIA NIH HHS/ Research Support, N.I.H., Extramural 2007/09/14 *J Comp Neurol*. 2007 Nov 10;505(2):190-208. doi: 10.1002/cne.21473.

[OAB19] K. Obernier and A. Alvarez-Buylla. Neural stem cells: origin, heterogeneity and regulation in the adult mammalian brain. *Development*, 146(4), 2019. Obernier, Kirsten Alvarez-Buylla, Arturo eng R01 HD032116/HD/NICHD NIH

HHS/ R01 NS028478/NS/NINDS NIH HHS/ R37 HD032116/HD/NICHD NIH HHS/ R37 NS028478/NS/NINDS NIH HHS/ Research Support, N.I.H., Extramural Research Support, Non-U.S. Gov't Review England 2019/02/20 Development. 2019 Feb 18;146(4):dev156059. doi: 10.1242/dev.156059.

[POAB13] G. Ponti, K. Obernier, and A. Alvarez-Buylla. Lineage progression from stem cells to new neurons in the adult brain ventricular-subventricular zone. *Cell Cycle*, 12(11):1649–50, 2013. Ponti, Giovanna Obernier, Kirsten Alvarez-Buylla, Arturo eng R37 HD032116/HD/NICHD NIH HHS/ Editorial 2013/05/16 Cell Cycle. 2013 Jun 1;12(11):1649-50. doi: 10.4161/cc.24984. Epub 2013 May 10.

[PVG<sup>+</sup>11] F. Pedregosa, G. Varoquaux, A. Gramfort, V. Michel, B. Thirion, O. Grisel, M. Blondel, P. Prettenhofer, R. Weiss, V. Dubourg, J. Vanderplas, A. Passos, D. Cournapeau, M. Brucher, M. Perrot, and E. Duchesnay. Scikit-learn: Machine learning in Python. *Journal of Machine Learning Research*, 12:2825–2830, 2011.

[QSS10] Alfio Quarteroni, Riccardo Sacco, and Fausto Saleri. *Numerical mathematics*, volume 37. Springer Science & Business Media, 2010.

[VGO<sup>+</sup>20] Pauli Virtanen, Ralf Gommers, Travis E. Oliphant, Matt Haberland, Tyler Reddy, David Cournapeau, Evgeni Burovski, Pearu Peterson, Warren Weckesser, Jonathan Bright, Stéfan J. van der Walt, Matthew Brett, Joshua Wilson, K. Jarrod Millman, Nikolay Mayorov, Andrew R. J. Nelson, Eric Jones, Robert Kern, Eric Larson, C J Carey, İlhan Polat, Yu Feng, Eric W. Moore, Jake VanderPlas, Denis Laxalde, Josef Perktold, Robert Cimrman, Ian Henriksen, E. A. Quintero, Charles R. Harris, Anne M. Archibald, Antônio H. Ribeiro, Fabian Pedregosa, Paul van Mulbregt, and SciPy 1.0 Contributors. SciPy 1.0: Fundamental Algorithms for Scientific Computing in Python. *Nature Methods*, 17:261–272, 2020.